THE JOURNAL OF BIOLOGICAL CHEMISTRY VOL. 285, NO. 48, pp. 37503–37512, November 26, 2010
Printed in the U.S.A.

AMP-activated Protein Kinase (AMPK) Negatively Regulates Nox4-dependent Activation of p53 and Epithelial Cell Apoptosis in Diabetes*[S]

Received for publication, April 21, 2010, and in revised form, August 30, 2010 Published, JBC Papers in Press, September 22, 2010, DOI 10.1074/jbc.M110.136796

Assaad A. Eid[‡], Bridget M. Ford[‡], Karen Block[‡§], Balakuntalam S. Kasinath[‡§], Yves Gorin[‡], Goutam Ghosh-Choudhury[‡§¶], Jeffrey L. Barnes[‡§], and Hanna E. Abboud[‡§1]

From the [‡]Department of Medicine, University of Texas Health Science Center, San Antonio, Texas 78229-3900 and [§]Veterans Affairs Research and [¶]Geriatric Research Education and Clinical Center, South Texas Veterans Healthcare System, San Antonio, Texas 78229

Diabetes and high glucose (HG) increase the generation of NADPH oxidase-derived reactive oxygen species and induce apoptosis of glomerular epithelial cells (podocytes). Loss of podocytes contributes to albuminuria, a major risk factor for progression of kidney disease. Here, we show that HG inactivates AMP-activated protein kinase (AMPK), up-regulates Nox4, enhances NADPH oxidase activity, and induces podocyte apoptosis. Activation of AMPK blocked HG-induced expression of Nox4, NADPH oxidase activity, and apoptosis. We also identified the tumor suppressor protein p53 as a mediator of podocyte apoptosis in cells exposed to HG. Inactivation of AMPK by HG up-regulated the expression and phosphorylation of p53, and p53 acted downstream of Nox4. To investigate the mechanism of podocyte apoptosis *in vivo*, we used OVE26 mice, a model of type 1 diabetes. Glomeruli isolated from these mice showed decreased phosphorylation of AMPK and enhanced expression of Nox4 and p53. Pharmacologic activation of AMPK by 5-aminoimidazole-4-carboxamide-1-riboside in OVE26 mice attenuated Nox4 and p53 expression. Administration of 5-aminoimidazole-4-carboxamide-1-riboside also prevented renal hypertrophy, glomerular basement thickening, foot process effacement, and podocyte loss, resulting in marked reduction in albuminuria. Our results uncover a novel function of AMPK that integrates metabolic input to Nox4 and provide new insight for activation of p53 to induce podocyte apoptosis. The data indicate the potential therapeutic utility of AMPK activators to block Nox4 and reactive oxygen species generation and to reduce urinary albumin excretion in type 1 diabetes.

One of the major early features of diabetic kidney disease is injury to glomerular epithelial cells or podocytes, which contribute to the increased urinary albumin losses and accelerated sclerosis of the glomerular microvascular bed (1). Podocyte injury manifests as phenotypic changes that range from foot process effacement and altered localization or abundance of specific slit diaphragm proteins to frank apoptosis with detachment of the cells from the glomerular basement membrane (GBM)[2] with decreased cell density (2–4). The mechanism(s) of podocyte depletion in diabetes are poorly understood.

Expression of antioxidant enzymes in some animal models ameliorates diabetic kidney disease, thus establishing a role of reactive oxygen species (ROS) (5, 6). More recently, along with ROS generated from mitochondrial respiratory chains, NADPH oxidase-derived ROS have been shown to play a significant role in injury to various organs, including the kidney (2, 7). A number of homologs of the phagocyte NADPH oxidase catalytic subunit (Nox2) have been identified. These enzymes participate in a number of biological processes, including proliferation, migration, contraction, cytoskeletal organization, fibrosis, and apoptosis (8). Along with Nox2, Nox1 and Nox4 are abundantly expressed in the renal cortex (9). We showed that Nox4 is expressed in rat and mouse glomeruli and contributes to matrix accumulation in diabetic kidney disease (2, 7). Abundant expression of Nox4 in glomerular podocytes has been reported (2, 10). High glucose (HG) increases the expression of Nox4 and NADPH oxidase activity in podocytes (2). However, the mechanism by which glucose increases NADPH oxidase activity and the role of Nox4 in podocyte apoptosis are not known.

AMP-activated protein kinase (AMPK), a serine/threonine kinase, is an energy sensor whose activity is regulated by glucose (11). AMPK is a heterotrimeric protein consisting of a catalytic α-subunit and regulatory β- and γ-subunits (12–15). Seven AMPK genes encoding two α (α1 and α2), two β (β1 and β2), and three γ (γ1, γ2, and γ3) isoforms are present in the mammalian genome (16–18). The activity and subunit composition of AMPK are expressed in a cell- and tissue-specific manner, with the α_1- and α_2-subunits expressed in the kidney and in

* This work was supported, in whole or in part, by National Institutes of Health Grants CA131272 (to K. B.), R01 DK079996 (to Y. G.), R01 DK50190 (to G. G.-C.), R01 DK080106 (to J. L. B.), and DK-R01-078971 (to H. E. A.) and George O'Brien Kidney Center-Morphology Core Grant DK061597 (to J. L. B.). This work was also supported by a National Kidney Foundation postdoctoral fellowship grant and a Juvenile Diabetes Research Foundation grant (to A. A. E.), a Juvenile Diabetes Research Foundation regular research grant (to Y. G.), and a Juvenile Diabetes Research Foundation grant and a Veterans Affairs merit review grant (to H. E. A.).

[S] The on-line version of this article (available at http://www.jbc.org) contains supplemental Figs. S1–S3.

[1] To whom correspondence should be addressed: Dept. of Medicine, Div. of Nephrology, MC 7882, University of Texas Health Science Center, 7703 Floyd Curl Dr., San Antonio, TX 78229-3900. Tel.: 210-567-4700; Fax: 210-567-4712; E-mail: abboud@uthscsa.edu.

[2] The abbreviations used are: GBM, glomerular basement membrane; ROS, reactive oxygen species; HG, high glucose; AMPK, AMP-activated protein kinase; DN, dominant-negative; AICAR, 5-aminoimidazole-4-carboxamide-1-riboside; ARA, adenine 9-β-D-arabinofuranoside; NG, normal glucose.

glomerular cells (19). Activation of AMPK requires phosphorylation of a critical threonine residue (Thr^{172}) in the activation loop of the α-subunit (20). In energy depletion states, AMPK activation slows metabolic reactions that consume ATP and stimulates reactions that produce ATP, thereby restoring the AMP/ATP ratio and the normal cellular energy stores (21). AMPK can also be activated independently of changes in the AMP/ATP ratio (22–24). AMPK signaling modulates multiple biological pathways, such as protein synthesis (25–27), autophagy (28, 29), and apoptosis (30–33).

In this study, we provide the first evidence that inactivation of AMPK by HG increases the expression of Nox4 and that the increased expression of Nox4 mediates podocyte apoptosis. Additionally, we demonstrate that Nox4 increases the abundance of p53 protein concomitant with an increase in its phosphorylation at Ser^{46} to increase the expression of the pro-apoptotic protein PUMA (p53-up-regulated modulator of apoptosis). In type 1 diabetic mice, AMPK is inactivated and up-regulates Nox4 to induce podocyte apoptosis. Furthermore, we show that pharmacologic activation of AMPK prevents these changes *in vitro* in podocytes and *in vivo* in diabetic mice and attenuates albuminuria.

EXPERIMENTAL PROCEDURES

Podocyte Culture and Transfection—Conditionally immortalized mouse podocytes, kindly provided by Dr. Katalin Susztack (Albert Einstein College of Medicine, Bronx, NY), were cultured as described previously (2). For the RNA interference experiments, a SMARTpool consisting of siRNA duplexes specific for mouse LKB1 or mouse p53 was obtained from Dharmacon. The SMARTpool of siRNAs was introduced into the cells by double transfection using Oligofectamine or Lipofectamine 2000 as described previously (34). The siRNAs for LKB1 and p53 were used at a concentration of 100 nM. Scrambled siRNAs (nontargeting siRNAs; 100 nM) served as controls to validate the specificity of the siRNAs. A replication-defective adenoviral vector encoding a truncated form of Nox4 lacking the NADPH-binding domain (referred to as AdDN-Nox4), a generous gift from Dr. Barry Goldstein (Thomas Jefferson University, Philadelphia, PA), was amplified in HEK293 cells. A GFP adenoviral vector control (referred to as AdGFP) was used as a control virus. Infection of cultured podocytes was carried out for 48 h. Wild-type active AMPKα2 (WT-AMPKα2) or dominant-negative AMPKα2 (DN-AMPKα2) plasmid constructs were procured from Addgene (35). Podocytes were transfected with 1.0 μg of WT-AMPKα2, DN-AMPKα2, or vector plasmid constructs using Lipofectamine 2000.

Animal Models—22-Week-old control FVB mice and OVE26 mice (FVB background; The Jackson Laboratory, Bar Harbor, ME) were used. At 17 weeks of age, OVE26 mice were treated with aminoimidazole-4-carboxamide-1-riboside 5-aminoimidazole-4-carboxamide-1-riboside (AICAR; 750 mg/kg/day) administered by intraperitoneal route (36). Before treatment with AICAR, mice were placed in metabolic cages for urine collection. Urine albumin was measured using a mouse albumin ELISA quantification kit (Bethyl Laboratories) and expressed as micrograms of albumin/24 h. Animals are killed by exsanguination under anesthesia. Both kidneys were removed and weighed. A slice of kidney cortex at the pole was embedded in paraffin or flash-frozen in liquid nitrogen for microscopy and image analyses. Cortical tissue was used for isolation of glomeruli by differential sieving with minor modifications as described previously (2, 37).

NADPH Oxidase Activity—NADPH oxidase activity was measured in podocytes grown in serum-free medium or in glomeruli isolated from kidney cortex as described previously (2, 7). Cultured podocytes were washed five times with ice-cold phosphate-buffered saline and scraped from the plate in the same solution, followed by centrifugation at 800 × *g* for 10 min at 4 °C. The cell pellets were resuspended in lysis buffer (20 mM KH_2PO_4 (pH 7.0), 1 mM EGTA, 1 mM phenylmethylsulfonyl fluoride, 10 μg/ml aprotinin, and 0.5 μg/ml leupeptin). Cell suspensions or washed glomeruli were homogenized with 100 strokes in a Dounce homogenizer on ice. To start the assay, 20 μg of homogenates was added to 50 mM phosphate buffer (pH 7.0) containing 1 mM EGTA, 150 mM sucrose, 5 μM lucigenin, and 100 μM NADPH. Photon emission expressed as relative light units was measured every 20 or 30 s for 10 min in a luminometer. A buffer blank (<5% of the cell signal) was subtracted from each reading. Superoxide production was expressed as relative light units/min/mg of protein. Protein content was measured using the Bio-Rad protein assay reagent.

AMPK Activity Assay—AMPK activity was measured using the AMPK KinEASE™ FP fluorescein green assay fluorescence polarization assay (Millipore) according to the manufacturer's protocol.

LKB1 Activity Assay—Endogenous LKB1 was immunoprecipitated with an antibody against LKB1 (Abcam, Cambridge, MA) and protein G beads. The reaction was initiated by the addition of 100 μl of kinase buffer containing 1 mM ATP, 10 μCi of [^{32}P]ATP (PerkinElmer Life Sciences), and 300 μm LKBtide (Upstate) into tubes containing the immunoprecipitated sample. After incubation at 30 °C for 10 or 20 min, the supernatant was applied to P81 paper (Whatman), and ^{32}P incorporation was determined by liquid scintillation counting.

Western Blot Analysis—Homogenates from glomeruli isolated from renal cortex were prepared in 200 μl of radioimmunoprecipitation assay buffer (20 mM Tris-HCl (pH 7.5), 150 mM NaCl, 5 mM EDTA, 1 mM Na_3VO_4, 1 mM phenylmethylsulfonyl fluoride, 20 μg/ml aprotinin, 20 μg/ml leupeptin, and 1% Nonidet P-40) using a Dounce homogenizer. Homogenates were incubated for 1 h at 4 °C and centrifuged at 10,000 × *g* for 30 min at 4 °C. Mouse podocytes were grown to near confluency in 60- or 100-mm dishes and serum-deprived for 24 h. All incubations were carried out in serum-free RPMI 1640 medium containing 0.2% BSA (fatty acid-free) at 37 °C for a specified duration. The cells were lysed in radioimmunoprecipitation assay buffer at 4 °C for 30 min. The cell lysates were centrifuged at 10,000 × *g* for 30 min at 4 °C. Protein in the supernatants was measured using the Bio-Rad method. For immunoblotting, proteins (30–60 μg) were separated by 12.5% SDS-PAGE and transferred to polyvinylidene difluoride membranes. Blots were incubated with rabbit polyclonal anti-Nox4 (1:1000; Novus Biologicals), rabbit monoclonal phospho-Thr^{172} AMPKα (40H9; 1:1000; Cell Signaling), rabbit polyclonal anti-AMPKα (1:1000; Cell Signaling), rabbit monoclonal phospho-

Ser^{428} LKB1 (C67A3; 1:1000; Cell Signaling), rabbit polyclonal LKB1 (1:1000; Abcam), and rabbit polyclonal anti-p53 (1:1000; Cell Signaling) antibodies. The primary antibodies were detected using horseradish peroxidase-conjugated IgG (1:2500 or 1:5000). Bands were visualized by enhanced chemiluminescence. Densitometric analysis was performed using NIH Image software.

mRNA Analysis—mRNA was analyzed by real-time RT-PCR using the $\Delta\Delta C_t$ method. Total RNA was isolated from cultured mouse podocytes or isolated glomeruli using the RNeasy® minikit (Qiagen). mRNA expression was quantified using the Mastercycler *realplex* (Eppendorf, Westbury, NY) with SYBR Green dye and predesigned mouse RT^2-quantitative PCR primers (SABiosciences, Frederick, MD) for Nox4 (RefSeq ID NM_015760), Trp53 (RefSeq ID NM_011640), and PUMA (RefSeq ID NM_133234) and normalized to β-actin (RefSeq ID NM_007393).

Apoptosis Assays and Cellular DNA Fragmentation—The cellular DNA fragmentation ELISA (Roche Diagnostics GmbH, Mannheim, Germany) for detection of BrdU-labeled DNA fragments in culture supernatants and cell lysates was used according to the manufacturer's protocol.

Apoptosis Assays, Annexin V, and Propidium Iodide Staining—An annexin V-FITC apoptosis detection kit (Calbiochem) was used for annexin V and propidium iodide staining according to the manufacturer's protocol. The percentage of apoptotic and necrotic cells was assessed by FACS (San Antonio Cancer Institute Core Facility at University of Texas Health Science Center, San Antonio, TX).

Apoptosis Assays and Caspase-3 Activity—A caspase-3 fluorescence assay kit (Cayman Chemical Co.) was used according to the manufacturer's protocol.

Electron Microscopy—Kidney cortex was cut into 0.5–1-mm^3 pieces and fixed overnight in cold 4% formaldehyde and 1% glutaraldehyde in phosphate buffer and then embedded in Epon 812 resin. 0.50-mm plastic sections were cut and stained with toluidine blue for identification of representative areas for subsequent sectioning using an ultramicrotome. Ultrathin sections were stained with uranyl acetate and examined and photographed on a JEOL 100CX electron microscope. All EM photomicrographs were examined in a blind fashion. Individual capillary loops were examined and quantified in five glomeruli/group of animals for the degree of foot process effacement as described by Jo *et al.* (38). The procedure adopted for GBM thickening measurement was a modification of the harmonic mean method summarized by Dische (39) and adapted from Jensen *et al.* (40) and Hirose *et al.* (41) as described in detail by Carlson *et al.* (42).

Podocyte Enumeration—Dual-label immunohistochemistry was used to identify and count glomerular epithelial cells relative to the GBM using a modification of methods described previously (43). To identify podocytes, 3-μm frozen sections of kidney cortex on glass slides were stained with anti-synaptopodin antibody, followed by Cy3-labeled donkey anti-goat IgG. After washing and to identify the GBM, the sections were stained with a rabbit antibody directed against collagen type IV, followed by FITC-labeled donkey anti-rabbit IgG. After staining and washing, the sections were preserved on coverslips in Prolong® gold antifade mounting medium with DAPI (Invitrogen) for fluorescence detection of nuclei. Sections were examined by epifluorescence using excitation and band-pass filters optimal for FITC, Cy3, and DAPI. Digital images representing each fluorochrome were taken of random glomeruli using an Olympus AX70 research microscope and a DP70 digital camera. 25–35 glomerular cross-sections per animal were photographed in each color channel, providing a minimum of 100 composite images per experimental group. The images were merged and color-balanced using Image-Pro Plus imaging software (Media Cybernetics, Inc., Silver Spring, MD), and podocytes were counted in projected images in a blind fashion by two individuals. Synaptopodin-positive cells on the outer aspect of the GBM were considered glomerular epithelial cells and counted. Synaptopodin-negative cells or cells in the inner aspect of the GBM were not counted. The mean area of each glomerular profile was measured manually, tracing the glomerular outline, encircling the area of interest, and calculating the surface area by computerized morphometry using MetaMorph Version 4.69 (2, 44, 45).

Statistical Analysis—Results are expressed as the mean ± S.E. Statistical significance was assessed by Student's unpaired *t* test. Significance was determined as $p < 0.05$.

RESULTS

Nox4 Mediates Apoptosis Induced by HG—The mechanism by which glucose increases NADPH oxidase activity, whether it involves AMPK, and the role of Nox4 in podocyte apoptosis are is not known. As expected, exposure of mouse podocytes to 25 mM HG for 12, 24, and 48 h significantly increased apoptosis as measured by annexin V binding (supplemental Fig. S1*A*), caspase-3 activation (supplemental Fig. S1*B*), and cellular DNA fragmentation (supplemental Fig. S1*C*). An equimolar concentration of mannitol had no effect (supplemental Fig. S1, *B* and *C*). Impairment of Nox4 function using an adenovirus encoding a dominant-negative form of the enzyme (AdDN-Nox4) significantly inhibited NADPH oxidase activity (Fig. 1*A*) and dramatically reduced HG-induced annexin V binding (Fig. 1*B*), caspase-3 activity (Fig. 1*C*), and cellular DNA fragmentation (Fig. 1*D*). These results demonstrate that Nox4-derived ROS mediate apoptosis of podocytes induced by HG.

HG Decreases the Phosphorylation of LKB1 and AMPK—Exposure of mouse podocytes to 25 mM glucose decreased AMPKα phosphorylation at its activating site, Thr^{172} (supplemental Fig. S2*A*), concomitant with reduction in AMPK activity (supplemental Fig. S2*B*). To elucidate the mechanism by which HG inhibits AMPK, we tested the effect of HG on the phosphorylation and activity of LKB1, an upstream kinase that phosphorylates AMPK at Thr^{172} (46). HG decreased LKB1 phosphorylation at Ser^{428} (supplemental Fig. S2*C*), a phosphorylation site required for metformin-enhanced AMPK activation (47). HG also decreased LKB1 activity (supplemental Fig. S2*D*). To determine whether the effect of HG on AMPK is mediated by LKB1, podocytes were transfected with siRNA targeting LKB1 prior to treatment with AICAR and HG. In cells incubated with HG, treatment with AICAR restored LKB1 and AMPKα phosphorylation, whereas siRNA targeting LKB1 reversed the effect of AICAR on the phosphorylation of LKB1 and AMPKα

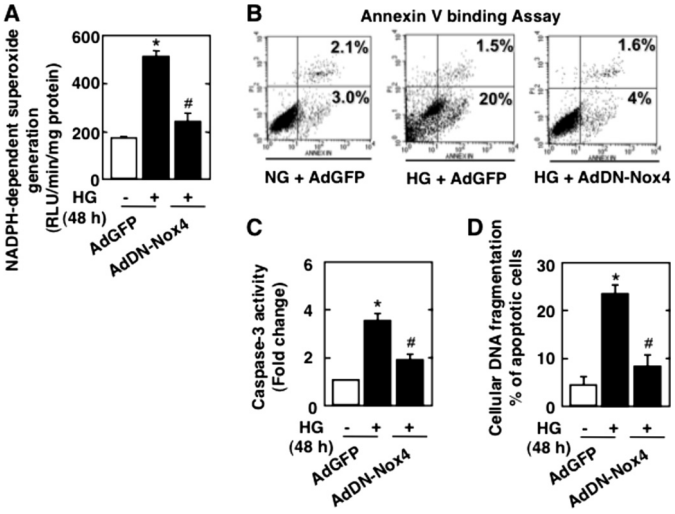

FIGURE 1. **NADPH oxidase Nox4 mediates HG-induced podocyte apoptosis.** Podocytes were infected with AdDN-Nox4 or AdGFP and treated with either HG (25 mmol/liter) or NG (5 mmol/liter) for 48 h. *A*, NADPH-dependent superoxide generation measured in podocytes infected with AdGFP and treated with NG or HG or in podocytes transfected with AdDN-Nox4 and treated with HG. *RLU*, relative light units. *B*, percent annexin V-positive cells 48 h after infection with AdGFP or AdDN-Nox4 in HG. *C*, ELISA for cellular DNA fragmentation. *D*, histogram representing caspase-3 activity. All values are the mean ± S.E. from four independent experiments. *, $p < 0.05$ *versus* the control; #, $p < 0.05$ *versus* HG treatment.

(supplemental Fig. S3). These data indicate that the effect of HG in inhibiting AMPK phosphorylation and activity is at least partially due to reduction in LKB1 phosphorylation and activity.

AMPK Regulates Nox4-dependent Podocyte Apoptosis—To determine whether inactivation of AMPKα mediates HG-induced Nox4 expression and apoptosis, podocytes were exposed to HG in the absence or presence of the AMPKα activator AICAR. Cells in normal glucose were also incubated with the AMPKα inhibitor adenine 9-β-D-arabinofuranoside (ARA). In cells incubated with HG, treatment with AICAR restored AMPKα phosphorylation at Thr^{172} (Fig. 2*A*) as well as AMPK activity (Fig. 2*B*). AICAR treatment also prevented the increase in Nox4 mRNA (Fig. 2*C*) and protein expression (Fig. 2*D*) and significantly blocked NADPH oxidase activity in response to HG (Fig. 2*E*). On the other hand, treatment of cells incubated in normal glucose (NG) with the AMPK inhibitor ARA mimicked the effect of HG and reduced AMPKα phosphorylation (Fig. 2*A*) and activity (Fig. 2*B*). Also, ARA resulted in up-regulation of Nox4 mRNA (Fig. 2*C*) and protein (Fig. 2*D*) and enhanced NADPH oxidase activity (Fig. 2*E*) in cells incubated with NG.

In parallel experiments, podocytes were transfected with a plasmid overexpressing wild-type AMPKα2 prior to exposure to HG, or cells in NG were transfected with a plasmid overexpressing dominant-negative AMPKα2. Expression of AMPKα2 restored AMPKα phosphorylation (Fig. 2*F*) and AMPK activity (Fig. 2*G*) and reduced HG-induced Nox4 mRNA (Fig. 2*H*) and protein expression (Fig. 2*I*) as well as NADPH oxidase activity (Fig. 2*J*), similar to the effect of AICAR. In contrast, in podocytes incubated with NG, the expression of dominant-negative AMPKα2 inhibited phosphorylation and activation of AMPK (Fig. 2, *F* and *G*), enhanced expression of Nox4 mRNA (Fig. 2*H*) and protein (Fig. 2*I*), and increased NADPH oxidase activity (Fig. 2*J*), similar to the effects of ARA. These data clearly implicate inactivation of AMPK by HG in the increased expression of Nox4 mRNA and protein and NADPH oxidase activation.

We next examined the role of AMPK in apoptosis of podocytes induced by HG. HG significantly augmented annexin V binding, caspase-3 activation, and DNA fragmentation (Fig. 3, *A–C*). Incubation of podocytes with the AMPK activator AICAR significantly inhibited HG-induced apoptosis (Fig. 3, *A–C*), whereas the pharmacologic AMPK inhibitor ARA mimicked the effect of HG and induced apoptosis of podocytes in NG (Fig. 3, *A–C*). To confirm the pharmacologic effect of the AMPK activator and inhibitor, wild-type or dominant-negative AMPKα2 was expressed in podocytes. As observed with AICAR, expression of AMPKα2 inhibited HG-induced annexin V binding, caspase-3 activation, and DNA fragmentation (Fig. 3, *D–F*). On the other hand, expression of dominant-negative AMPKα2 in podocytes incubated in NG induced significant apoptosis compared with control cells (Fig. 3, *D–F*). These results indicate that AMPK inactivation by HG mediates podocyte apoptosis.

p53 Regulates HG-induced Podocyte Apoptosis—To determine the mechanism by which HG induces podocyte apoptosis, we considered the role of the p53 tumor suppressor protein, which influences cell survival in a cell type- and context-dependent manner (48, 49). Treatment of podocytes with HG increased the expression of p53 mRNA (Fig. 4*A*) and protein (Fig. 4*B*) levels and enhanced p53 phosphorylation at the activating site, Ser^{46} (Fig. 4*B*). p53 induced the expression of many pro-apoptotic genes, including PUMA. HG increased PUMA mRNA levels in podocytes (Fig. 4*C*). siRNA-mediated down-regulation of p53 mRNA and protein (Fig. 4, *A* and *B*) markedly decreased PUMA mRNA levels (Fig. 4*C*). Moreover, p53 siRNA prevented podocyte apoptosis as assessed by annexin V binding (Fig. 4*D*), caspase-3 activity (Fig. 4*E*), and cellular DNA fragmentation (Fig. 4*F*). These results indicate a role for p53 in the pro-apoptotic effect of HG on podocytes.

AMPK/Nox4 Axis Regulates HG-induced p53—We have shown above that HG-induced podocyte apoptosis resulted from AMPK inactivation and Nox4-derived ROS production (Figs. 1 and 3). We tested the role of AMPK and Nox4 on p53 in cells stimulated with HG. Incubation of podocytes with the AMPK activator AICAR decreased the expression of p53 protein and its serine phosphorylation in cells exposed to HG (Fig. 5*A*). AICAR also decreased the expression of PUMA protein and mRNA (Fig. 5, *A* and *B*). Conversely, the AMPK inhibitor ARA augmented p53 protein levels, serine phosphorylation of p53 (Fig. 5*A*), and PUMA protein and mRNA levels in cells incubated in NG (Fig. 5, *A* and *B*), mimicking the effect of HG. The pharmacologic effects of AICAR and ARA were confirmed using wild-type AMPKα2 and dominant-negative AMPKα2. Expression of wild-type AMPKα2 decreased HG-induced expression and phosphorylation of p53 (Fig. 5*C*) and attenuated PUMA protein and mRNA expression (Fig. 5, *C* and *D*). On the other hand, expression of dominant-negative AMPKα2 in cells incubated in NG increased p53 protein levels, p53 phosphorylation, and PUMA protein and mRNA expression (Fig. 5, *C* and *D*).

We next examined the role of Nox4 in p53 activation. Inhibition of Nox4 using AdDN-Nox4 attenuated HG-induced expression of p53 protein and its serine phosphorylation (Fig. 5*E*). Furthermore, inhibition of Nox4 abolished the expression

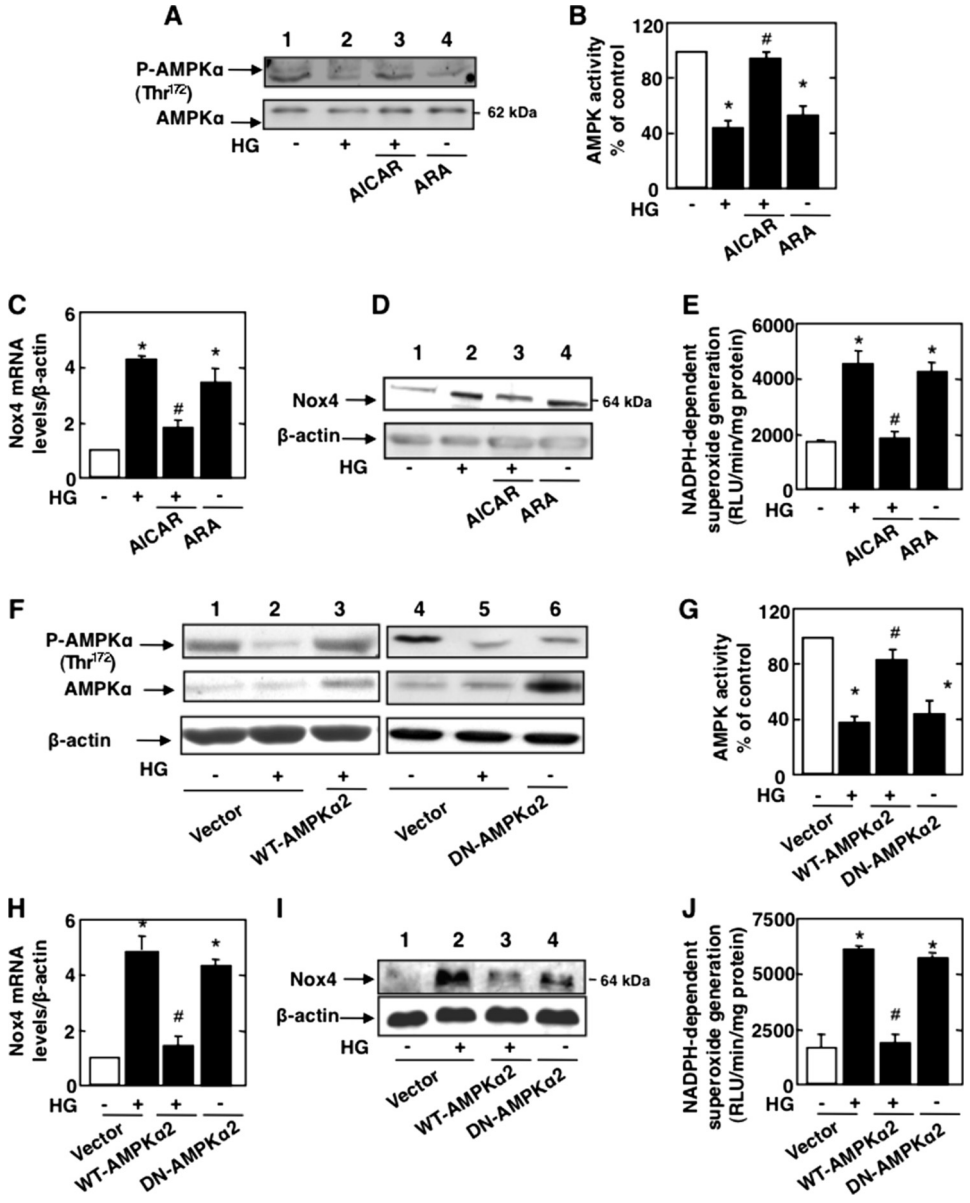

FIGURE 2. **AMPK regulates Nox4-dependent podocyte apoptosis.** Podocytes were exposed either to HG (25 mmol/liter) with or without AICAR (1 mmol/liter) or to ARA (1 mmol/liter) in NG (5 mmol/liter) for 48 h. *A*, representative Western blot of phospho-Thr^{172} AMPKα and AMPKα. *B*, histogram representing AMPK activity measured in podocytes treated with HG and AICAR or treated with ARA in NG. *C*, relative mRNA levels of Nox4 in control and treated podocytes. *D*, representative Western blot of Nox4 and β-actin levels. *E*, NADPH-dependent superoxide generation measured in podocytes treated with HG and AICAR or treated with ARA in NG. In parallel experiments, podocytes were transfected with WT-AMPKα2 in HG or transfected with DN-AMPKα2 in NG. *RLU*, relative light units. *F* and *G*, WT-AMPKα2 in the presence of HG increases phospho-Thr^{172} AMPKα expression and AMPK activity, respectively. Shown is a representative Western blot of phospho-Thr^{172} AMPKα and AMPKα (*F*) and a histogram representing AMPK activity measured in podocytes transfected with WT-AMPKα2 and treated with HG or transfected with DN-AMPKα2 in NG (*G*). *H*, relative mRNA levels of Nox4. *I*, representative Western blot of Nox4 and β-actin levels. *J*, NADPH-dependent superoxide generation measured in podocytes transfected with WT-AMPKα2 and treated with HG or transfected with DN-AMPKα2 in NG. All values are the mean $\pm$ S.E. from four independent experiments. *, $p < 0.05$ *versus* the control; #, $p < 0.05$ *versus* HG treatment.

of PUMA protein and mRNA (Fig. 5, *E* and *F*). These data indicate that AMPK and its downstream effector Nox4 regulate the expression/phosphorylation of the transcription factor p53 and its target, the pro-apoptotic protein PUMA.

AMPK Inactivation Up-regulates Nox4 and Enhances NADPH Oxidase Activity and p53 Expression in Type 1 Diabetes—To determine the *in vivo* relevance of the findings in cultured cells, type 1 diabetic OVE26 mice were treated with the AMPK activator AICAR for 5 weeks. Control FVB mice were treated with vehicle. OVE26 mice display elevated blood glucose levels compared with control FVB mice. OVE26 mice treated with AICAR had equivalent levels of blood glucose compared with untreated OVE26 mice (Table 1). Body weight was significantly reduced in OVE26 mice and in OVE26 mice treated with AICAR compared with their FVB littermates. Total kidney weight and kidney/body weight ratio, indices of renal hypertrophy, increased significantly in OVE26 mice compared with FVB littermates. Renal hypertrophy in OVE26 mice treated with AICAR was significantly reduced compared with untreated OVE26 mice (Table 1). AMPK phosphorylation (Fig. 6*A*) and activity (Fig. 6*B*) were reduced in OVE26 compared with FVB mouse glomeruli (Fig. 6, *A* and *B*), whereas Nox4 protein levels (Fig. 6*C*) and NADPH oxidase activity (Fig. 6*D*) were increased. These parameters were restored to control levels when OVE26 mice were treated with AICAR (Fig. 6, *A–D*).

The activation of apoptotic pathways was also examined in glomeruli of OVE26 mice. In these mice, the levels of p53 were significantly increased compared with control FVB mice (Fig. 6*E*), together with increased expression of PUMA protein and mRNA (Fig. 6, *E* and *F*). Treatment of diabetic mice with AICAR reduced p53 expression (Fig. 6*E*) as well as the expression of PUMA protein and mRNA (Fig. 6, *E* and *F*). These results demonstrate that in type 1 diabetes, inactivation of AMPK results in enhanced Nox4 expression and NADPH oxidase activity, with a subsequent increase in the expression of p53 and its pro-apoptotic target, PUMA.

AMPK Regulates GBM Thickening, Foot Process Effacement, Podocyte Loss, and Albuminuria in Type 1 Diabetic Mice—Electron microscopic analysis revealed a significant increase in GBM thickening in OVE26 mice compared with control FVB littermates (Fig. 7, *A*, compare *panel b* with *panel a*, *blue arrows*; and *B*). Marked effacement of foot processes was evident in diabetic mice (Fig. 7, *A* and *C*). Also, diabetic OVE26 mice lost podocytes as judged by the number of synaptopodin-

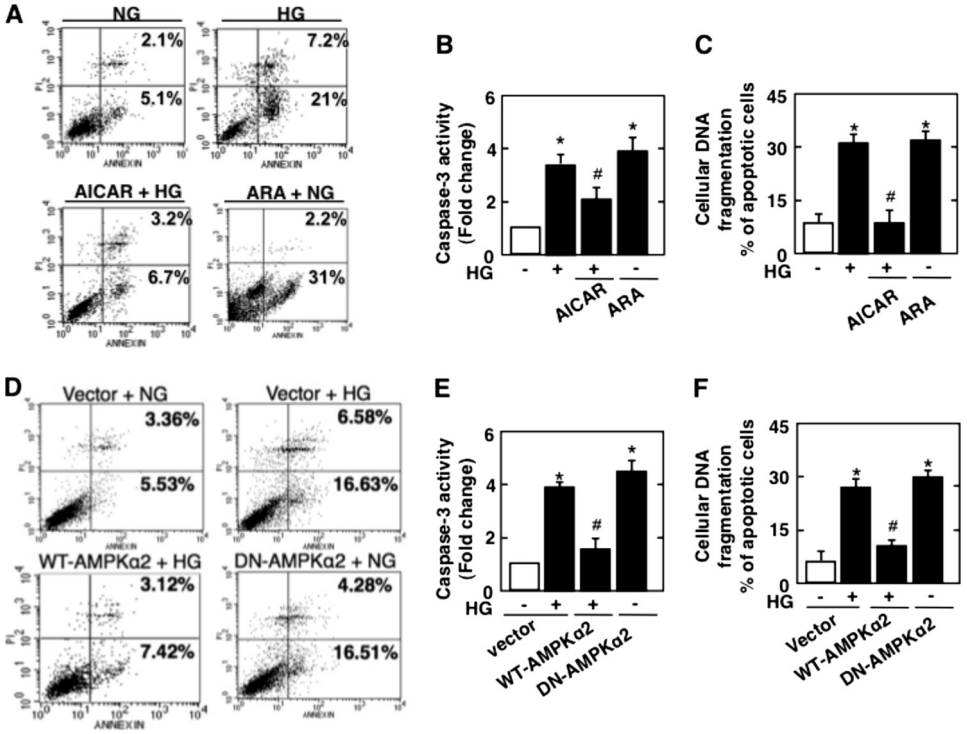

FIGURE 3. **AMPK regulates HG-induced podocyte apoptosis.** Mouse podocytes were serum-deprived for 24 h and pretreated with the AMPK activator AICAR (1 mmol/liter) for 1 h before incubation with HG or were incubated with the AMPK inhibitor ARA (1 mmol/liter) in the presence of NG for 48 h. In parallel experiments, mouse podocytes were transfected with WT-AMPKα2 before treatment with HG or transfected with DN-AMPKα2 in NG. AICAR treatment inhibited HG-induced apoptosis, whereas ARA induced apoptosis as measured by annexin V binding (*A*), caspase-3 activity (*B*), and cellular DNA fragmentation (*C*). The effect of HG on podocyte apoptosis was also blocked by WT-AMPKα2 and reproduced by DN-AMPKα2 in NG medium as measured by annexin V binding (*D*), caspase-3 activity (*E*), and cellular DNA fragmentation (*F*). All values are the mean ± S.E. from four independent experiments. *, $p < 0.05$ *versus* the control; #, $p < 0.05$ *versus* HG.

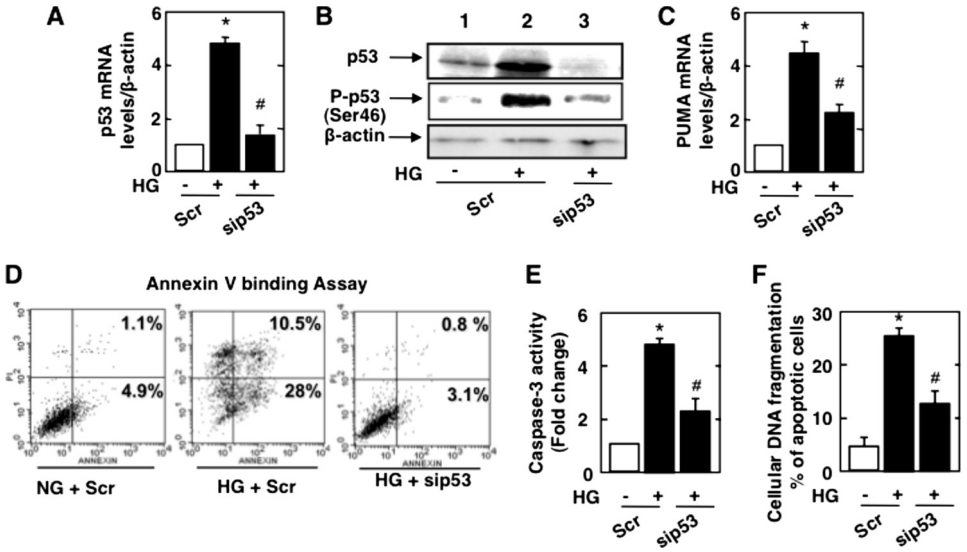

FIGURE 4. **p53 mediates HG-induced podocyte apoptosis.** Mouse podocytes were transfected with scrambled siRNA (nontargeting; *Scr*) or with siRNA for p53 (*sip53*) in NG or HG. *A*, relative mRNA amount of p53. *B*, representative Western blot of p53, phospho-Ser^{46} p53, and β-actin. *C*, relative mRNA amount of PUMA in podocytes transfected with scrambled siRNA in NG or HG or transfected with p53 siRNA and treated with HG. *D*, percent annexin V-positive cells 48 h after transfection with scrambled or p53 siRNA in HG. *E* and *F*, histograms of caspase-3 activity and ELISA for cellular DNA fragmentation, respectively. All values are the mean ± S.E. from four independent experiments. *, $p < 0.05$ *versus* the control + Scr; #, $p < 0.05$ *versus* HG + Scr.

positive cells in the glomeruli (Fig. 7, *D*, *red* staining; and *E*). Importantly, treatment of the diabetic mice with AICAR resulted in a significant decrease in foot process effacement (Fig. 7, *A* and *C*) and GBM thickening (Fig. 7, *A* and *B*) and prevented podocyte loss (Fig. 7, *D* and *E*). FVB, OVE26, and AICAR-treated OVE26 mice were placed in metabolic cages for 24 h. Urine was collected, and albumin levels were measured. Treatment of diabetic mice with AICAR resulted in a significant decrease in albumin excretion compared with control untreated diabetic mice (Fig. 7*F*). These data confirm the observations in the cultured podocytes and indicate that inactivation of AMPK and the increase in Nox4 expression play a critical role in podocyte injury and albuminuria in type 1 diabetes.

DISCUSSION

Podocyte apoptosis is an early glomerular phenotype that contributes to podocyte depletion, albuminuria, and progression of renal disease (2, 50). In this study, we have provided the first evidence that podocyte apoptosis in diabetes is mediated through inactivation of AMPK, up-regulation of Nox4, and an increase in NADPH oxidase-mediated ROS production. Furthermore, we have demonstrated that AMPK and Nox4 regulate the expression/phosphorylation of p53 and the pro-apoptotic protein PUMA. We have also shown that the AMPK/Nox4-driven pro-apoptotic pathway is operative in glomeruli of diabetic mice and that activation of AMPK by the administration of AICAR attenuates Nox4 and p53 expression, reduces albuminuria, and protects mice against podocyte loss and glomerular injury (Fig. 8).

ROS-generating NADPH oxidases play a dual role in regulating cellular apoptosis (8, 51–53). NADPH-generated ROS play an important role in ethanol-induced apoptosis (51). However, NADPH oxidase-derived ROS, including Nox4, inhibit apoptosis in pancreatic cancer cells (52, 53). In this study, we have demonstrated that Nox4 induces podocyte apoptosis and identify inactivation of AMPK as a mechanism by which HG and hyperglycemia increase the expression of Nox4.

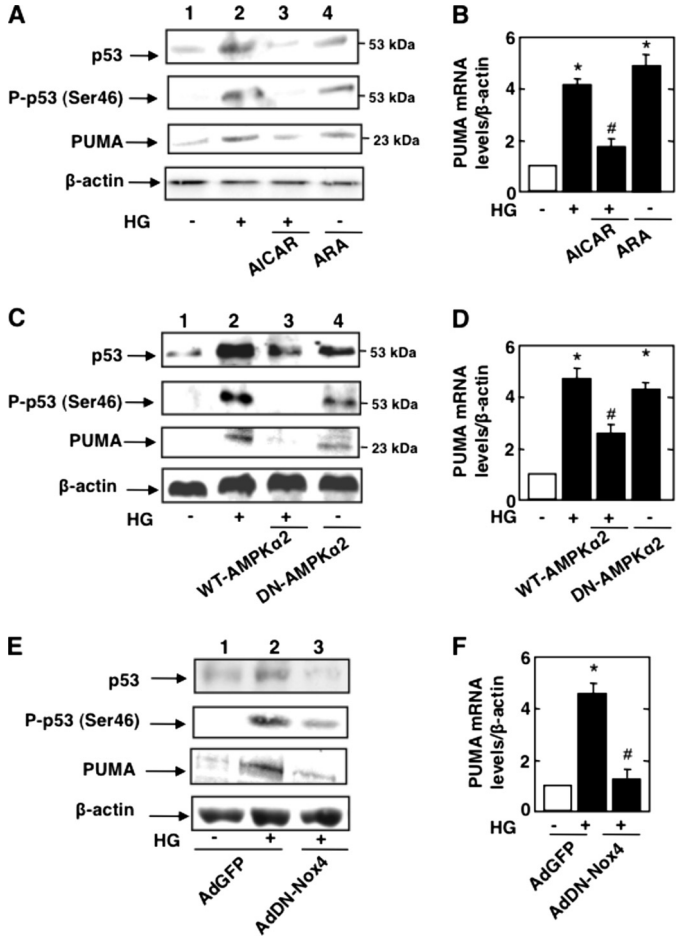

FIGURE 5. **AMPK/Nox4 axis regulates HG-induced p53 and PUMA.** Mouse podocytes were serum-deprived for 24 h and pretreated with the AMPK activator AICAR (1 mmol/liter) for 1 h before incubation with HG, or mouse podocytes were incubated with the AMPK inhibitor ARA (1 mmol/liter) in the presence of NG for 48 h. *A*, representative Western blot of p53, phospho-Ser[46] p53, PUMA, and β-actin. *B*, relative mRNA levels of PUMA. In parallel experiments, mouse podocytes were transfected with WT-AMPKα2 before treatment with HG or transfected with DN-AMPKα2 in NG. *C*, representative Western blot of p53, phospho-Ser[46] p53, PUMA, and β-actin levels. *D*, relative mRNA levels of PUMA. In an another set of experiments, podocytes were infected with AdDN-Nox4 or AdGFP in NG or HG. *E*, representative Western blot of p53, phospho-Ser[46] p53, PUMA, and β-actin. F, relative mRNA levels of PUMA. All values are the mean ± S.E. from four independent experiments. *, $p < 0.05$ *versus* the control; #, $p < 0.05$ *versus* HG treatment.

TABLE 1

Glucose level, body weight, kidney weight, and kidney weight/body weight ratio of FVB control mice, OVE26 type 1 diabetic mice, and OVE26 mice treated with AICAR

Values are the means ± S.E. from five animals for each group.

Group	*n*	Blood glucose	Body weight	Kidney weight	Kidney weight/ body weight
		mg/dl	*g*	*g*	*g/kg*
FVB	5	148 ± 14.3	23 ± 1.2	0.21 ± 0.02	8.7 ± 0.8
OVE26	5	570 ± 28.5[a]	18 ± 0.9[a]	0.25 ± 0.04[a]	13.8 ± 0.6[a]
OVE26 + AICAR	5	563 ± 31.2	19 ± 1.8	0.20 ± 0.03[b]	9.7 ± 0.7[b]

[a] $p < 0.05$, OVE26 mice *versus* FVB mice.
[b] $p < 0.05$, OVE26 mice treated with AICAR compared with OVE26 mice.

AMPK activity is maintained through constitutive phosphorylation of Thr[172] in the catalytic α-subunit by such upstream kinases as LKB1 and calcium/calmodulin kinase kinase-β (20, 22–24). The interaction between ROS and AMPK is regulated

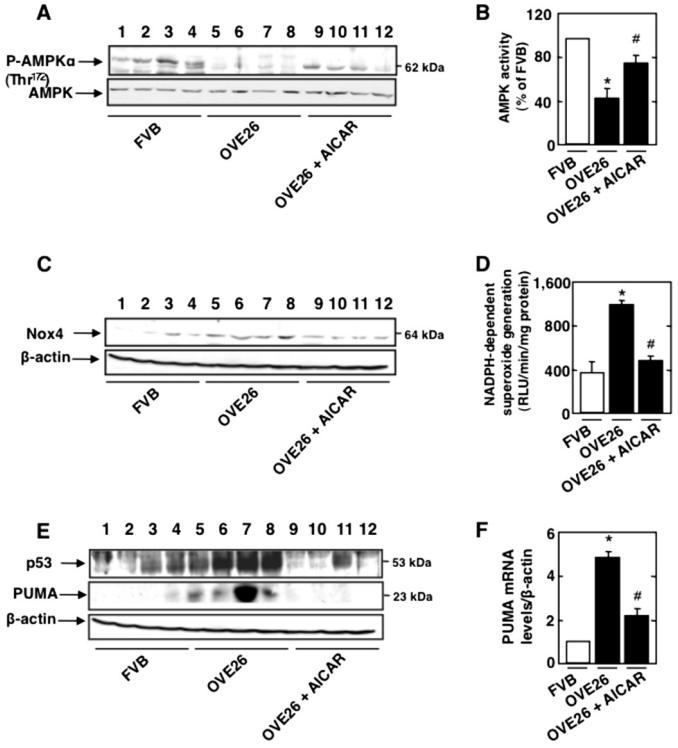

FIGURE 6. **AMPK inactivation up-regulates Nox4 and enhances NADPH oxidase activity and p53 expression in type 1 diabetic mice.** 17-week-old OVE26 mice were treated with AICAR (750 mg/kg/day, dissolved in saline, intraperitoneal) for 5 weeks. Mice in the control group received saline vehicle. Glomeruli were isolated from the kidneys of three groups of mice ($n = 5$): control FVB mice, OVE26 mice, and OVE26 mice treated with AICAR. *A*, representative Western blot of phospho-Thr[172] AMPKα and total AMPKα of four of five mice from each group (FVB mice, *lanes 1–4*; OVE26 mice, *lane 5–8*; and OVE26 mice treated with AICAR, *lanes 9–12*). *B*, histogram of AMPK activity. *C*, representative Western blot of Nox4 and β-actin of four mice of five from each group (FVB mice, *lanes 1–4*; OVE26 mice, *lane 5–8*; and OVE26 mice treated with AICAR, *lanes 9–12*). *D*, NADPH-dependent superoxide generation. *RLU*, relative light units. *E*, representative Western blot of p53, PUMA, and β-actin of four mice of five from each group (FVB mice, *lanes 1–4*; OVE26 mice, *lane 5–8*; and OVE26 mice treated with AICAR, *lanes 9–12*). *F*, relative amount of PUMA mRNA. *, $p < 0.05$, OVE26 mice *versus* FVB mice; #, $p < 0.05$, OVE26 mice treated with AICAR compared with OVE26 mice treated with vehicle.

in a cell stimulus- and tissue-specific manner. During hypoxia, mitochondria-generated ROS activate AMPK (54). Similarly, during exercise, NADPH oxidase-derived ROS induce AMPK activation (55). However, in β-cells exposed to HG, AMPK activation increases ROS production and potentiates β-cell apoptosis (56). AMPK plays a role in renal cell injury (10, 27). Type 1 diabetic rats treated with AICAR, a pharmacologic activator of AMPK, show significant attenuation of renal hypertrophy (27). Inhibition of AMPK activity *in vitro* alters localization of ZO-1 (zona occludens-1) in podocytes, an effect reversed by the pharmacologic activator AICAR and by the AMPK activator adiponectin (10), indicating a role for this stress-sensing kinase in podocyte biology.

AMPK exerts pro- or anti-apoptotic effects that are stimulus- or cell type-specific (30–33). In pancreatic β-cells, HG activates AMPK and enhances the production of ROS, resulting in loss of mitochondrial membrane potential (56). On the other hand, in umbilical vein endothelial cells, activation of AMPK increases the expression of the antioxidant manganese superoxide dismutase and inhibits HG-induced intracellular and

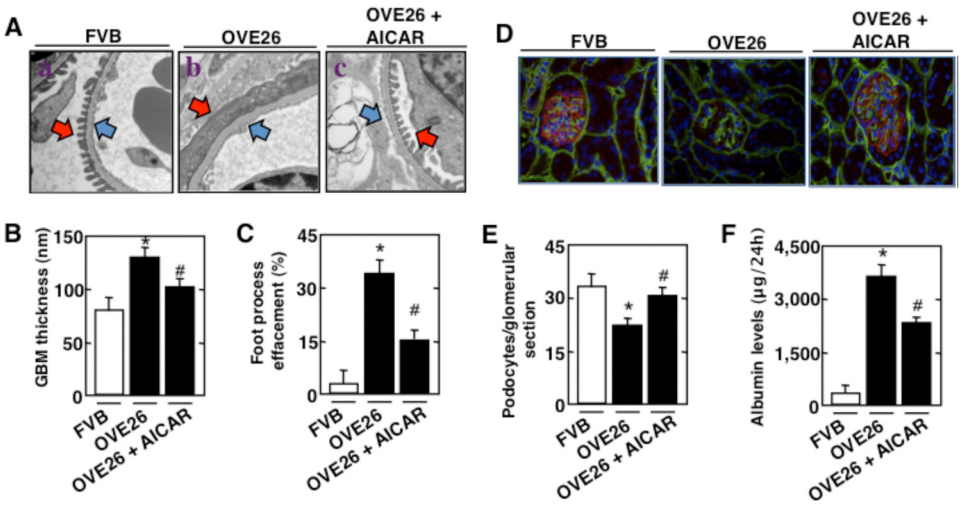

FIGURE 7. **AMPK regulates GBM thickening, foot process effacement, podocyte loss, and albuminuria in type 1 diabetic mice.** 17-week-old OVE26 mice were treated with AICAR (750 mg/kg/day, dissolved in saline, intraperitoneal) for 5 weeks. Mice in the control group received saline vehicle. Glomeruli were isolated from the kidneys of three groups of mice ($n = 5$): control FVB mice, OVE26 mice, and OVE26 mice treated with AICAR. *A*, representative transmission electron micrographs of glomerular cross-sections of FVB, OVE26, and AICAR-treated OVE26 mice. The images show foot process effacement (*panel b*, *red arrow*), cytoplasmic rarefaction, and basement membrane thickening (*panel b*, *blue arrow*) of an OVE26 mouse. This effect was not seen in OVE26 mice treated with AICAR (*panel c*). *B*, histogram representing thickness of the GBM measured in nanometers. *C*, semiquantitative analysis of foot process effacement of glomeruli from each group of animals. *D*, representative immunofluorescent images of glomeruli stained with collagen IV (*green*), synaptopodin (*red*), and DAPI (*blue*). *E*, barogram representing podocyte number per glomerular section. *, $p < 0.05$, OVE26 mice *versus* FVB mice; #, $p < 0.05$, AICAR-treated OVE26 mice compared with OVE26 mice. *F*, FVB, OVE26, and AICAR-treated OVE26 mice were placed in metabolic cages for 24 h. Urine was collected, and albumin levels were measured and expressed as micrograms of albumin/24 h. Values are the mean ± S.E. *, $p < 0.05$, OVE26 mice *versus* control FVB mice; #, $p < 0.05$, decrease in albumin levels in AICAR-pretreated OVE26 mice *versus* untreated OVE26 mice (n = five per group).

mitochondrial ROS production (57), suggesting that activated AMPK may suppress oxidative stress. The data in our study demonstrate that HG inactivates AMPK and significantly increases the expression of Nox4 and NADPH oxidase activity. Activation of AMPK by AICAR or expression of the AMPKα2 subunit prevents these effects of HG. Our data also suggest that inhibition of AMPK by HG is likely due to reduction in the phosphorylation and activity of LKB1. These results are consistent with recently published data showing that AMPK inactivation by HG is due to reduced LKB1 activity (58).

In this study, we also established that inactivation of AMPK increases Nox4 and NADPH oxidase activity and mediates the pro-apoptotic effect of HG on podocytes. In fact, our results using the pharmacologic activator AICAR or the inhibitor ARA indicate that AMPK inactivation is necessary for podocyte apoptosis. This conclusion is further substantiated using exogenous AMPKα2 and dominant-negative AMPKα2. To our knowledge, this is the first report in which inactivation of AMPK is linked to increased expression of Nox4 and NADPH oxidase activity, resulting in cell apoptosis in the HG environment. However, the mechanism by which AMPK regulates Nox4 protein expression and whether it involves transcription or stabilization of the mRNA need to be explored.

The active tumor suppressor transcription factor p53 is induced by genotoxic stress and energy starvation, both of which promote cell death (49). It plays a compelling role in the apoptotic intrinsic pathway by integrating the action of pro-apoptotic Bax (Bcl-2-associated X protein) (49). This action of p53 is regulated mainly by enhanced transcription of Bax (48). However, a direct transcription-independent role of p53 in the induction of apoptosis has also been reported (59, 60). Also, p53 directly activates the pro-apoptotic protein Bax to initiate apoptosis through the mitochondrial pathway (60). In this study, HG induced caspase-3 activation and DNA fragmentation and apoptosis of podocytes in culture. The induction of apoptosis by HG was associated with a significant increase in p53 mRNA and protein. Furthermore, down-regulation of p53 blocked HG-induced apoptosis of podocytes. These results represent a mechanism of HG-induced podocyte apoptosis involving p53 plausibly through the intrinsic pathway.

Phosphorylation of p53 at multiple serine residues is required for its transcriptional activity (48). Phosphorylation at Ser^{46} correlates with the p53 transcriptional program that launches apoptosis (61, 62). Kinases such as PKCδ and p38 MAPK, which may phosphorylate this residue, are known to be activated by HG (48, 63–65). Our results demonstrate that HG increases p53 phosphorylation at Ser^{46}, suggesting enhancement of its transcriptional activity. We also observed an increase in p53 protein levels in cells exposed to HG. Therefore, it is likely that the increase in p53 phosphorylation is an indirect effect resulting from increased p53 levels.

The transcription-dependent pro-apoptotic function of p53 is mediated principally by the pro-apoptotic protein Bax and the BH3-only protein PUMA, either of which can carry out apoptosis through the mitochondrial pathway (65). PUMA-deficient mice show a requirement of p53-dependent PUMA expression for induction of apoptosis in many tissues (65, 66). Interestingly, this function of PUMA establishes that both transcription-dependent and transcription-independent activities of p53 are required for induction of apoptosis (48). PUMA binds to the anti-apoptotic protein Bcl-x_L, thus releasing cytosolic p53 to activate Bax (48, 60). In this study, we have shown a HG-mediated increase in the expression of PUMA mRNA concomitant with enhanced accumulation and phosphorylation of p53. Also, we have shown that PUMA expression is dependent upon HG-induced expression of p53. Furthermore, HG significantly enhanced the expression of Bax in podocytes (data not shown). These results suggest that HG stimulates accumulation of p53, which contributes to apoptosis of podocytes likely through the intrinsic pathway.

AMPK has been shown to regulate p53 activity and phosphorylation in a stimulus- and tissue-specific manner. Nutrient-deprived thymocytes show enhanced apoptosis associated with an increase in AMPK activity. In this model, AMPK activation

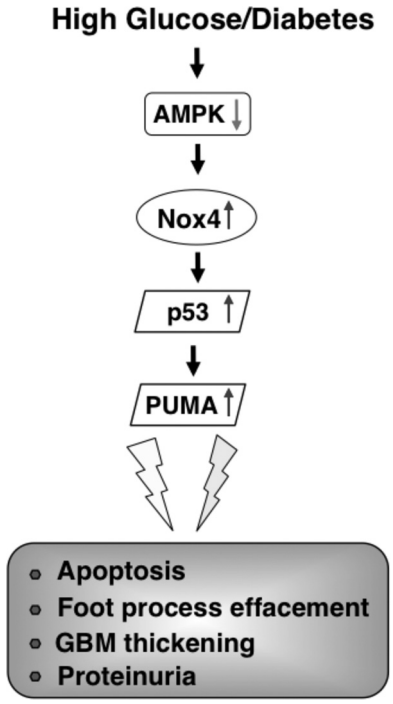

FIGURE 8. **Proposed mechanism of HG/diabetes-induced glomerular epithelial cell (podocyte) apoptosis.** See "Discussion" for details.

results in enhanced levels of p53 and its Ser^{46} phosphorylation (67). In murine embryonic fibroblasts, low glucose also activates AMPK and induces the expression and phosphorylation of p53 (68). Furthermore, glucose starvation reduces p53 stability, which correlates with AMPK inactivation, indicating that AMPK may positively regulate the function of p53 (69). In this study, we found that podocytes cultured in NG had low levels of p53. Treatment with HG significantly increased p53 mRNA and protein levels and p53 phosphorylation. We also showed that pharmacologic and genetic activation of AMPK inhibited the accumulation of p53 and its phosphorylation in response to HG. In addition, our data demonstrate that inactivation of AMPK by ARA exerts effects similar to HG and induces the expression and phosphorylation of p53, resulting in enhanced expression of PUMA mRNA and protein. Collectively, our data indicate that in podocytes, AMPK negatively regulates p53 expression/phosphorylation and expression of the pro-apoptotic protein PUMA.

The interaction between p53 and ROS is well described (70). p53 has been shown to regulate ROS generation, and conversely, ROS generation modulates selective transactivation of p53 target genes (70). In our study, we have presented evidence that Nox4 regulates the expression and phosphorylation of p53 in response to HG and that Nox4 mediates HG-induced expression of PUMA. These results conclusively demonstrate a positive regulatory role of inactivated AMPK and up-regulated Nox4 in the increased expression and phosphorylation of p53, leading to apoptosis of podocytes exposed to HG.

We previously reported glomerular hypertrophy and increased matrix protein expression in type 1 diabetic rats concomitant with increased Nox4 expression; inhibition of Nox4 ameliorates glomerular hypertrophy and matrix expansion (7). More recently, we reported increased expression of Nox4 in glomeruli of diabetic OVE26 mice (2). In this study, we have provided evidence that increased expression of Nox4 and augmented NADPH oxidase activity in glomeruli of these diabetic mice are associated with podocyte loss and severe albuminuria. *In vitro*, our results show involvement of AMPK inactivation in the up-regulation of Nox4, which results in enhanced expression of p53 necessary for podocyte apoptosis in cells exposed to HG (Figs. 2–5). In line with these data, we found that pharmacologic activation of AMPK in diabetic OVE26 mice resulted in attenuation of Nox4 expression and a decrease in NADPH oxidase activity. AMPK inactivation in diabetic OVE26 mice also increased the expression of p53 in the glomeruli and enhanced the expression of the pro-apoptotic PUMA mRNA and protein (Fig. 6, *E* and *F*). These results indicate that Nox4-mediated up-regulation of p53 and PUMA may contribute to the loss of podocytes in the diabetic glomeruli (Fig. 7, *D* and *E*) and that activation of AMPK by the administration of AICAR attenuates Nox4 expression and podocyte loss and ameliorates albuminuria.

Although the contribution of ROS to the complications of diabetic kidney disease is established, the administration of antioxidants has not been associated with potent protection against apoptosis in human diabetic nephropathy (71). Our data in this study identify a previously unrecognized direct target, Nox4, for treating diabetic kidney disease. Our observations suggest that AMPK activators or Nox4 inhibitors may represent an adjunct therapy in addition to metabolic control to reduce kidney damage in type 1 diabetes.

Acknowledgments—We thank Andrea Barrantine, Sergio Garcia, and Fredyne Springer for technical assistance.

REFERENCES

1. de Zeeuw, D., Remuzzi, G., Parving, H. H., Keane, W. F., Zhang, Z., Shahinfar, S., Snapinn, S., Cooper, M. E., Mitch, W. E., and Brenner, B. M. (2004) *Kidney Int.* **65,** 2309–2320
2. Eid, A. A., Gorin, Y., Fagg, B. M., Maalouf, R., Barnes, J. L., Block, K., and Abboud, H. E. (2009) *Diabetes* **58,** 1201–1211
3. Kanwar, Y. S., Liu, Z. Z., Kumar, A., Usman, M. I., Wada, J., and Wallner, E. I. (1996) *J. Clin. Invest.* **98,** 2478–2488
4. Wolf, G., Chen, S., and Ziyadeh, F. N. (2005) *Diabetes* **54,** 1626–1634
5. Brownlee, M. (2001) *Nature* **414,** 813–820
6. DeRubertis, F. R., Craven, P. A., and Melhem, M. F. (2007) *Metabolism* **56,** 1256–1264
7. Gorin, Y., Block, K., Hernandez, J., Bhandari, B., Wagner, B., Barnes, J. L., and Abboud, H. E. (2005) *J. Biol. Chem.* **280,** 39616–39626
8. Lassègue, B., and Griendling, K. K. (2010) *Arterioscler. Thromb. Vasc. Biol.* **30,** 653–661
9. Gill, P. S., and Wilcox, C. S. (2006) *Antioxid. Redox Signal.* **8,** 1597–1607
10. Sharma, K., Ramachandrarao, S., Qiu, G., Usui, H. K., Zhu, Y., Dunn, S. R., Ouedraogo, R., Hough, K., McCue, P., Chan, L., Falkner, B., and Goldstein, B. J. (2008) *J. Clin. Invest.* **118,** 1645–1656
11. Long, Y. C., and Zierath, J. R. (2006) *J. Clin. Invest.* **116,** 1776–1783
12. Hardie, D. G., and Carling, D. (1997) *Eur. J. Biochem.* **246,** 259–273
13. Hardie, D. G., Carling, D., and Halford, N. (1994) *Semin. Cell Biol.* **5,** 409–416
14. Kemp, B. E., Mitchelhill, K. I., Stapleton, D., Michell, B. J., Chen, Z. P., and Witters, L. A. (1999) *Trends Biochem. Sci.* **24,** 22–25
15. Mitchelhill, K. I., Stapleton, D., Gao, G., House, C., Michell, B., Katsis, F., Witters, L. A., and Kemp, B. E. (1994) *J. Biol. Chem.* **269,** 2361–2364

16. Rutter, G. A., Da Silva Xavier, G., and Leclerc, I. (2003) *Biochem. J.* **375,** 1–16
17. Carling, D. (2004) *Trends Biochem. Sci.* **29,** 18–24
18. Hardie, D. G. (2004) *J. Cell Sci.* **117,** 5479–5487
19. Cammisotto, P. G., and Bendayan, M. (2008) *J. Mol. Histol.* **39,** 579–584
20. Hawley, S. A., Davison, M., Woods, A., Davies, S. P., Beri, R. K., Carling, D., and Hardie, D. G. (1996) *J. Biol. Chem.* **271,** 27879–27887
21. Kahn, B. B., Alquier, T., Carling, D., and Hardie, D. G. (2005) *Cell. Metab.* **1,** 15–25
22. Woods, A., Dickerson, K., Heath, R., Hong, S. P., Momcilovic, M., Johnstone, S. R., Carlson, M., and Carling, D. (2005) *Cell. Metab.* **2,** 21–33
23. Hurley, R. L., Anderson, K. A., Franzone, J. M., Kemp, B. E., Means, A. R., and Witters, L. A. (2005) *J. Biol. Chem.* **280,** 29060–29066
24. Hawley, S. A., Pan, D. A., Mustard, K. J., Ross, L., Bain, J., Edelman, A. M., Frenguelli, B. G., and Hardie, D. G. (2005) *Cell. Metab.* **2,** 9–19
25. Shibata, R., Ouchi, N., Ito, M., Kihara, S., Shiojima, I., Pimentel, D. R., Kumada, M., Sato, K., Schiekofer, S., Ohashi, K., Funahashi, T., Colucci, W. S., and Walsh, K. (2004) *Nat. Med.* **10,** 1384–1389
26. Tian, R., Musi, N., D'Agostino, J., Hirshman, M. F., and Goodyear, L. J. (2001) *Circulation* **104,** 1664–1669
27. Lee, M. J., Feliers, D., Mariappan, M. M., Sataranatarajan, K., Mahimainathan, L., Musi, N., Foretz, M., Viollet, B., Weinberg, J. M., Choudhury, G. G., and Kasinath, B. S. (2007) *Am. J. Physiol. Renal Physiol.* **292,** F617–F627
28. Matsui, Y., Takagi, H., Qu, X., Abdellatif, M., Sakoda, H., Asano, T., Levine, B., and Sadoshima, J. (2007) *Circ. Res.* **100,** 914–922
29. Meijer, A. J., and Codogno, P. (2007) *Autophagy* **3,** 238–240
30. Hickson-Bick, D. L., Buja, L. M., and McMillin, J. B. (2000) *J. Mol. Cell. Cardiol.* **32,** 511–519
31. Russell, R. R., 3rd, Li, J., Coven, D. L., Pypaert, M., Zechner, C., Palmeri, M., Giordano, F. J., Mu, J., Birnbaum, M. J., and Young, L. H. (2004) *J. Clin. Invest.* **114,** 495–503
32. Kim, J., Ahn, J. H., Kim, J. H., Yu, Y. S., Kim, H. S., Ha, J., Shinn, S. H., and Oh, Y. S. (2007) *Exp. Eye Res.* **84,** 886–893
33. Riboulet-Chavey, A., Diraison, F., Siew, L. K., Wong, F. S., and Rutter, G. A. (2008) *Diabetes* **57,** 415–423
34. Gorin, Y., Ricono, J. M., Wagner, B., Kim, N. H., Bhandari, B., Choudhury, G. G., and Abboud, H. E. (2004) *Biochem. J.* **381,** 231–239
35. Mu, J., Brozinick, J. T., Jr., Valladares, O., Bucan, M., and Birnbaum, M. J. (2001) *Mol. Cell* **7,** 1085–1094
36. Lemieux, K., Konrad, D., Klip, A., and Marette, A. (2003) *FASEB J.* **17,** 1658–1665
37. Abboud, H. E., Ou, S. L., Velosa, J. A., Shah, S. V., and Dousa, T. P. (1982) *J. Clin. Invest.* **69,** 327–336
38. Jo, Y. I., Cheng, H., Wang, S., Moeckel, G. W., and Harris, R. C. (2007) *Nephron Exp. Nephrol.* **107,** e87–e94
39. Dische, F. E. (1992) *Arch. Pathol. Lab. Med.* **116,** 43–49
40. Jensen, E. B., Gundersen, H. J., and Osterby, R. (1979) *J. Microsc.* **115,** 19–33
41. Hirose, K., Osterby, R., Nozawa, M., and Gundersen, H. J. G. (1982) *Kidney Int.* **21,** 689–695
42. Carlson, E. C., Audette, J. L., Klevay, L. M., Nguyen, H., and Epstein, P. N. (1997) *Anat. Rec.* **247,** 9–19
43. Faulkner, J. L., Szcykalski, L. M., Springer, F., and Barnes, J. L. (2005) *Am. J. Pathol.* **167,** 1193–1205
44. Kim, Y. H., Goyal, M., Kurnit, D., Wharram, B., Wiggins, J., Holzman, L., Kershaw, D., and Wiggins, R. C. (2001) *Kidney Int.* **60,** 957–968
45. Sanden, S. K., Wiggins, J. E., Goyal, M., Riggs, L. K., and Wiggins, R. C. (2003) *J. Am. Soc. Nephrol.* **14,** 2484–2493
46. Hong, S. P., Leiper, F. C., Woods, A., Carling, D., and Carlson, M. (2003) *Proc. Natl. Acad. Sci. U.S.A.* **100,** 8839–8843
47. Xie, Z., Dong, Y., Scholz, R., Neumann, D., and Zou, M. H. (2008) *Circulation* **117,** 952–962
48. Vousden, K. H., and Prives, C. (2009) *Cell.* **137,** 413–431
49. Chipuk, J. E., and Green, D. R. (2006) *Cell Death Differ.* **13,** 994–1002
50. Susztak, K., Raff, A. C., Schiffer, M., and Böttinger, E. P. (2006) *Diabetes* **55,** 225–233
51. Dong, J., Sulik, K. K., and Chen, S. Y. (2010) *Toxicol. Lett.* **193,** 94–100
52. Vaquero, E. C., Edderkaoui, M., Pandol, S. J., Gukovsky, I., and Gukovskaya, A. S. (2004) *J. Biol. Chem.* **279,** 34643–34654
53. Mochizuki, T., Furuta, S., Mitsushita, J., Shang, W. H., Ito, M., Yokoo, Y., Yamaura, M., Ishizone, S., Nakayama, J., Konagai, A., Hirose, K., Kiyosawa, K., and Kamata, T. (2006) *Oncogene* **25,** 3699–3707
54. Emerling, B. M., Weinberg, F., Snyder, C., Burgess, Z., Mutlu, G. M., Viollet, B., Budinger, G. R., and Chandel, N. S. (2009) *Free Radic. Biol. Med.* **46,** 1386–1391
55. Moir, H., Hughes, M. G., Potter, S., Sims, C., Butcher, L. R., Davies, N. A., Verheggen, K., Jones, K. P., Thomas, A. W., and Webb, R. (2010) *J. Appl. Physiol.* **108,** 1284–1292
56. Kim, W. H., Lee, J. W., Suh, Y. H., Lee, H. J., Lee, S. H., Oh, Y. K., Gao, B., and Jung, M. H. (2007) *Cell. Signal.* **19,** 791–805
57. Kukidome, D., Nishikawa, T., Sonoda, K., Imoto, K., Fujisawa, K., Yano, M., Motoshima, H., Taguchi, T., Matsumura, T., and Araki, E. (2006) *Diabetes* **55,** 120–127
58. Lee, M., Feliers, D., Sataranatarajan, K., Mariappan, M. M., Li, M., Barnes, J. L., Choudhury, G. G., and Kasinath, B. S. (2010) *Cell. Signal.* **22,** 65–70
59. Mihara, M., Erster, S., Zaika, A., Petrenko, O., Chittenden, T., Pancoska, P., and Moll, U. M. (2003) *Mol. Cell* **11,** 577–590
60. Chipuk, J. E., Kuwana, T., Bouchier-Hayes, L., Droin, N. M., Newmeyer, D. D., Schuler, M., and Green, D. R. (2004) *Science* **303,** 1010–1014
61. D'Orazi, G., Cecchinelli, B., Bruno, T., Manni, I., Higashimoto, Y., Saito, S., Gostissa, M., Coen, S., Marchetti, A., Del Sal, G., Piaggio, G., Fanciulli, M., Appella, E., and Soddu, S. (2002) *Nat. Cell Biol.* **4,** 11–19
62. Hofmann, T. G., Möller, A., Sirma, H., Zentgraf, H., Taya, Y., Dröge, W., Will, H., and Schmitz, M. L. (2002) *Nat. Cell Biol.* **4,** 1–10
63. Geraldes, P., Hiraoka-Yamamoto, J., Matsumoto, M., Clermont, A., Leitges, M., Marette, A., Aiello, L. P., Kern, T. S., and King, G. L. (2009) *Nat. Med.* **15,** 1298–1306
64. Levine, A. J., Feng, Z., Mak, T. W., You, H., and Jin, S. (2006) *Genes Dev.* **20,** 267–275
65. Yu, J., and Zhang, L. (2003) *Cancer Cell* **4,** 248–249
66. Villunger, A., Michalak, E. M., Coultas, L., Müllauer, F., Böck, G., Ausserlechner, M. J., Adams, J. M., and Strasser, A. (2003) *Science* **302,** 1036–1038
67. Okoshi, R., Ozaki, T., Yamamoto, H., Ando, K., Koida, N., Ono, S., Koda, T., Kamijo, T., Nakagawara, A., and Kizaki, H. (2008) *J. Biol. Chem.* **283,** 3979–3987
68. Jones, R. G., Plas, D. R., Kubek, S., Buzzai, M., Mu, J., Xu, Y., Birnbaum, M. J., and Thompson, C. B. (2005) *Mol. Cell* **18,** 283–293
69. Lee, C. H., Inoki, K., Karbowniczek, M., Petroulakis, E., Sonenberg, N., Henske, E. P., and Guan, K. L. (2007) *EMBO J.* **26,** 4812–4823
70. Liu, B., Chen, Y., and St Clair, D. K. (2008) *Free Radic. Biol. Med.* **44,** 1529–1535
71. Forbes, J. M., Coughlan, M. T., and Cooper, M. E. (2008) *Diabetes* **57,** 1446–1454